Special Collection

Towards the Operational Window for Nitridic and Carbidic Palladium Nanoparticles for Directed Catalysis

Lucy G Costley-Wood,[a] Khaled Mohammed,[b] Marina Carravetta,[b] Donato Decarolis,[c, d] Alexandre Goguet,[e] Apostolos Kordatos,[b] Reza Vakili,[e] Haresh Manyar,[e] Erin McPake,[a] Chris-Kriton Skylaris,[b] Paul Thompson,[f] Emma K Gibson,*[a] and Peter P. Wells*[b, d]

The reactions under which interstitial structures of Pd form are profoundly important and prevalent in catalysis; the formation and stability of Pd hydride structures are well understood, however, interstitial structures of the carbide and nitride are relatively under explored. This work reports a systematic study of the formation and stability of PdC_x and PdN_x at elevated temperatures and different atmospheres using *in situ* Pd L_3 edge XANES spectroscopy. These studies were further complemented by the application of ^{14}N MAS-NMR experiments and computational DFT investigations. The experiments confirmed that PdC_x was significantly more stable than PdN_x; ^{14}N MAS-NMR provided direct confirmation on the formation of the nitride, however, the XANES studies evidenced very limited stability under the conditions employed. Moreover, the results suggest that the formation of the nitride imparts some structural changes that are not entirely reversible under the conditions used in these experiments. This work provides important insights into the stability of interstitial structures of Pd and the conditions in which they could be employed for directed catalytic processes.

Introduction

Supported Pd nanoparticles (NPs) underpin both existing and emerging industrial catalytic processes; from exhaust emission control technology[1,2] to directing the selective upgrading of bioderived feedstocks[3–6] to value-added chemicals.[7–10] However, these supported Pd NPs are dynamic, and are known to undergo significant changes under reaction conditions.[11–16] For example, the formation of new bulk and subsurface phases, which have profound consequences on the catalytic performance.[17–21]

Palladium carbide can be formed on exposure to CO and some hydrocarbons at elevated temperatures.[12,14,15,22–24] Carbon containing feed molecules adsorb onto the palladium, dissociate, and the carbon atoms are inserted into the FCC lattice of the reduced palladium particle.[12,25–28] DFT calculations by Garcia-Mota show carbide formation at surface step sites first.[29] Gradual dissolution of this carbon through the lattice initially causes a subsurface and eventually a bulk carbide like phase.[12,29] For alkyne semi-hydrogenation reactions, this PdC_x phase increases selectivity to the alkene, by inhibiting over-hydrogenation to the alkane.[12,13,18,22,29] This effect on selectivity is multifaceted. Firstly, the top most layers prevent hydrogen from populating the subsurface.[13] In addition, the mobility of existing dissolved hydrogen through a carbide phase to the surface is decreased.[22,12] Finally, the carbide phase increases the energy barrier of adsorption of further hydrocarbons from the feed.[29] At low conversions, a surface poisoning effect of the alkyne is also responsible for high selectivities.[18] Some demonstrations of this improved selectivity include the semi-hydrogenation of acetylene, propyne and 1-pentyne.[12,22,28,29]

Palladium hydride is also formed under reactive conditions, and has shown to influence selectivity.[13,15,22] In a similar manner to the formation of the carbide, the hydride is also formed by

[a] L. G Costley-Wood, E. McPake, Dr. E. K Gibson
School of Chemistry
University of Glasgow
Glasgow, G12 8QQ (UK)
E-mail: emma.gibson@glasgow.ac.uk
[b] Dr. K. Mohammed, Dr. M. Carravetta, Dr. A. Kordatos, Prof. C.-K. Skylaris, Dr. P. P. Wells
School of Chemistry
University of Southampton
Southampton, SO17 1BJ (UK)
E-mail: p.p.wells@soton.ac.uk
[c] Dr. D. Decarolis
Cardiff Catalysis Institute
School of Chemistry
Cardiff University
Cardiff, CF10 3AT (UK)
[d] Dr. D. Decarolis, Dr. P. P. Wells
UK Catalysis Hub
Research Complex at Harwell, Rutherford Appleton Laboratory, Harwell, Didcot, OX11 0FA (UK)
[e] Prof. A. Goguet, Dr. R. Vakili, Dr. H. Manyar
School of Chemistry and Chemical Engineering
Queen's University Belfast
Belfast, BT9 5AG (UK)
[f] P. Thompson
XMaS UK CRG Beamline
ESRF – The European Synchrotron
71, avenue des Martyrs, 38000 Grenoble (France)

Supporting information for this article is available on the WWW under https://doi.org/10.1002/cctc.202300870

This publication is part of a Special Collection on "Advanced Characterization Techniques in Catalysis"

the adsorption, dissociation, and insertion of hydrogen from the feed gas into reduced Pd nanoparticles.[15] Formation of the hydride is not only a function of reaction mixture stoichiometry but can also be influenced by the prehistory of the sample as evidenced by Teschner.[15] Under the same conditions where the carbide phase can form, the hydride phase can be promoted by increasing the H_2 partial pressure in the feed.[13,22] In contrast to PdC_x, the PdH_x increases selectivity to the alkane by increasing the availability of dissolved hydrogen.[12–14,22,28] However, the presence of the hydride is not a requirement for total hydrogenation of the alkyne to occur.[18] Furthermore, hydrogen can be present in the subsurface of the Pd NP from surface incorporation of carbonaceous deposits which contain hydrogen, not only from the feed mixture.[14]

The formation of bulk phase crystallographic palladium nitride has been attempted as far back as 1952, but successful synthesis and characterization of the interstitial structure comes from much more recent work.[30] Dann used X-ray absorption spectroscopy (XAS) at the Pd K and L_3 edges to follow the formation of a palladium nitride phase on a Pd/Al_2O_3 catalyst.[31] The PdN_x was formed *in situ* in a flow of NH_3 and O_2 in He, and also under NH_3 in He, at temperatures $< 200\,^{\circ}C$. Activity measurements by online mass spectroscopy (MS) showed that for the oxidation of ammonia, this PdN_x phase is responsible for high N_2 selectivity.[31]

Following this, Decarolis performed spatial profiling of the same catalyst during ammonia oxidation, using *operando* XAS at the Pd K edge and online MS to look at the structure-activity relationship during the reaction.[32] Enhanced selectivity to N_2 was observed when the PdN_x species was present, agreeing with the previous study. Under these conditions, multivariate curve resolution (MCR) analysis indicated a PdN_x phase, but also a bulk Pd(0) phase, suggesting the nitride structure may be limited to the surface and subsurface regions.[32]

The main technique used to study the nitride has been XAS at either the Pd K or L_3 edges.[31,32] XPS has also proved successful, and work by Dann was able to identify reduced nitrogen arising from bulk metal nitride at a different energy to the surface adsorbed NH_3 species.[31] Another method able to distinguish adsorbed and bulk nitrogen is solid-state magic angle spinning nuclear magnetic resonance spectroscopy (MAS-NMR). Nitrogen has two isotopes which are NMR active. ^{14}N has a natural abundance of 99.6% and an integer nuclear spin of 1, hence it has a nuclear quadrupolar interaction (NQI). Despite its low natural abundance, most NMR studies prefer ^{15}N, by means of expensive isotopic labelling, or with the use of dynamic nuclear polarization to increase the signal intensity. This is because ^{15}N is spin $^1/_2$ and therefore is not subject to the significant line broadening often associated with the NQI, which is often a major drawback in organic solids. In our target materials, nitrogen can form nitrides on the surface or in interstitial positions of the Pd nanoparticle. These two scenarios will result in variation in chemical shift, δ, which may be moderate, and variation on the local symmetry about the nitrogen, which will affect the NQI significantly. While ^{15}N NMR will only reveal chemical shift variations, ^{14}N NMR is much more powerful in this context as it is likely to allow discrimination between surface and interstitial nitrides. Moreover, metal nitrides are particularly amenable to ^{14}N NMR investigation as they have been reported to be often associated with sharp, well resolved signals as the nitrides occupy highly symmetric sites.

Clearly, the formation of Pd interstitial structures plays an important role in the performance of Pd catalysts.[17–18,20,28] So far, this influence on selectivity is limited to reactions under which conditions these structures can form and are stable. There is potential however to take advantage of these structures further and look at their formation as a pre-treatment in other common catalyzed reactions. In this study, we have used *in situ* XAS at the Pd L_3 edge to observe the formation of each of the palladium hydride, carbide and nitride on a Pd/Al_2O_3 catalyst. We have probed the stability of the carbide and nitride by exposing them to both inert and reducing atmospheres over a temperature range. Furthermore, solid state NMR calculations as well as MAS-NMR have been used to probe the nitrogen environment directly in Pd nitride, confirming the presence of interstitial nitrogen. Finally, we have applied Density Functional Theory (DFT) modelling to calculate the energy barriers for the decomposition of Pd nitride, via different mechanisms, and NMR electric field gradients.

Results and Discussion

Comparing interstitial structures

All experiments were performed using the same 1.5 wt % Pd on γ-alumina catalyst, that was prepared by standard incipient wetness impregnation of palladium nitrate, as described by Decarolis *et al.*[32] The preparation route yields well-dispersed particles with an average particle diameter of 2.1 nm.[31] Initially, the catalyst was exposed to three different sets of conditions to form palladium nitride, carbide and hydride, each on a fresh catalyst following a reductive pre-treatment; in brief, carbide was formed by exposure to C_2H_4/He at $200\,^{\circ}C$, nitride was formed with NH_3/He at $100\,^{\circ}C$, and hydride was produced by exposing the catalyst to H_2/He at $35\,^{\circ}C$. These experiments were performed *in situ* using a dedicated sample environment developed by the BM28 team at the ESRF and the resultant spectra collected at the Pd L_3 edge.[33–34] The L_3 edge (3.2 keV) was chosen for this experiment, rather than the more accessible K edge (24.3 keV). This softer edge, involving an electronic transition from a 2p to 4d state, is more sensitive to interstitial structures, with clear differences to the position and intensity of the white line on their formation.[12,31] For the hydride, an additional peak is also present at 3182 eV.[12,18,28,31]

Figure 1a) shows the spectra of all species, to our knowledge this is the first time all three interstitial structures have been formed and characterised on one sample. All species show a shift in energy of the white line compared to the metallic palladium foil. The shift is + 0.63 eV for PdH_x, +0.73 eV for PdN_x and +0.92 eV for PdC_x. This indicates structural changes to the palladium due to the incorporation of heteroatoms into the metal lattice.[31] The hydride also shows the additional characteristic peak, generated by an antibonding

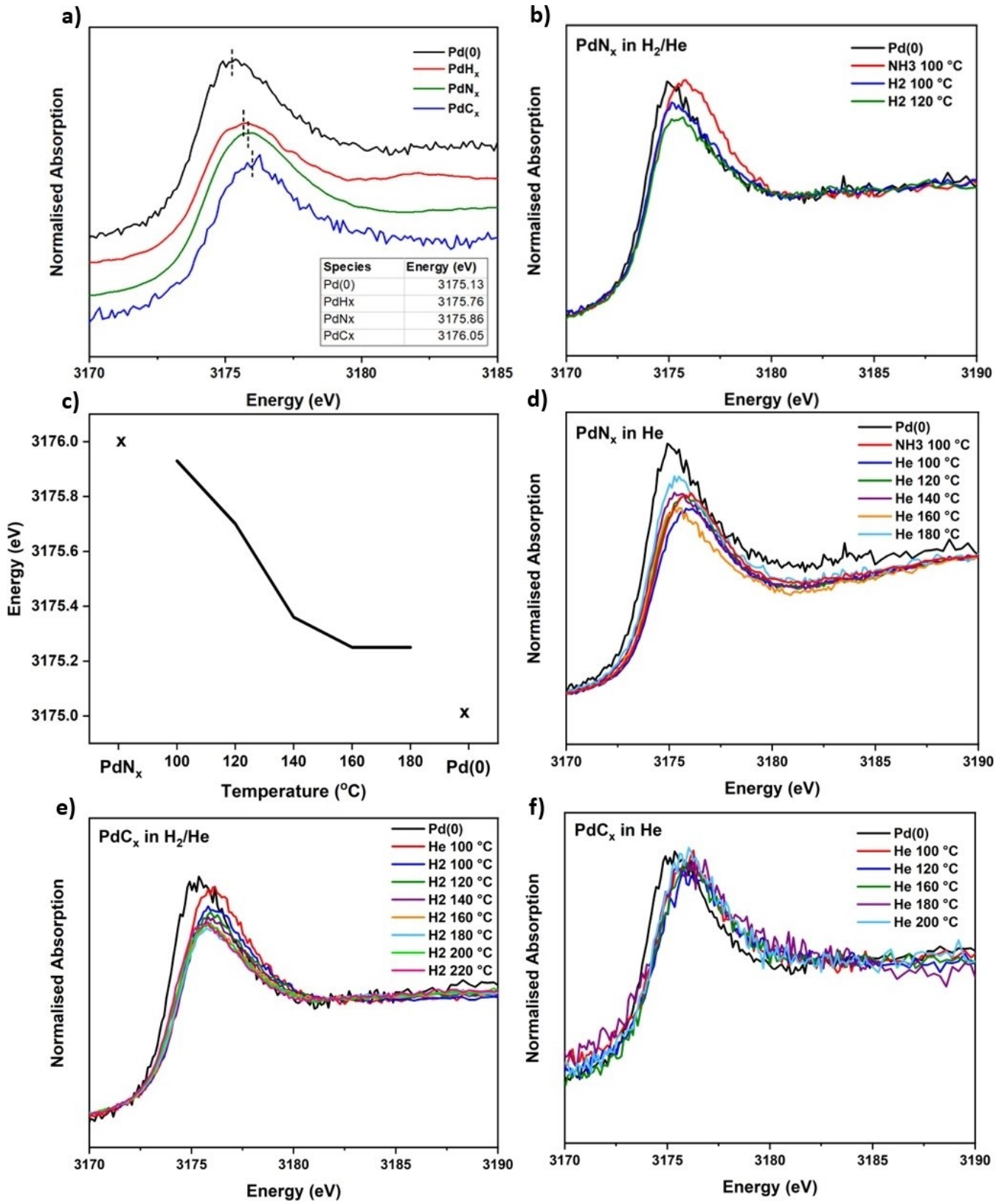

Figure 1. Pd L3-edge XANES spectra of: a) Pd(0), PdH_x, PdN_x and PdC_x, formed on a 1.5 wt% Pd/γ-Al_2O_3. b) PdN_x as pre-reduced Pd(0), nitrided PdN_x, and heated under H_2/He from 100–120 °C. c) Whiteline energy of species in figure d as a function of increasing temperature under He. Energy of assumed state at start, PdN_x, and end, Pd(0), are included. d) PdN_x as pre-reduced Pd(0), nitrided PdN_x, and heated under He only from 100–180 °C. e) PdC_x as pre-reduced Pd(0), carbided PdC_x, then heated under H_2/He from 100–220 °C. f) PdC_x as pre-reduced Pd(0), carbided PdC_x, then heated under He only from 100–200 °C.

Pd–H state formed from the overlap of a Pd *d*-orbital with a H *s*-orbital.[28] Interestingly, the spectra for PdN_x and PdC_x are almost identical at this energy. In the previous Pd L_3 investigation by Dann *et al.*, that assessed the evolving nature of Pd NPs during selective ammonia oxidation, the white line intensity of the nitride was greater than that reported here.[31] However, in the earlier work the Pd nitride spectrum was measured under ammonia oxidation conditions, and the increased white line intensity is most likely a consequence of a limited amount of oxygen adsorption. In fact, Decarolis identified a small PdO component to the bulk nitride phase in the work described above, where PdN_x was formed under identical conditions to this study.[32]

Formation of palladium hydride, PdH_x

Formation of PdH_x was achieved by cooling reduced Pd(0) to 35 °C under hydrogen. Whilst not investigated in this experiment, literature on the subject indicates the PdH_x decomposition temperature lies around 75 °C.[35] Furthermore, Nag found a correlation between structure, composition and decomposition temperature. The temperature range was found to be 55–75 °C, with temperature increasing as a result of both increasing Pd crystallite size and stoichiometric amount of hydrogen.[36]

Formation and stability of palladium nitride, PdN_x

To form palladium nitride, the catalyst was first reduced to Pd(0) in hydrogen, then exposed to 5% NH_3/He at 100 °C for 1 h. To test the thermal stability, the gas was then switched to either diluted hydrogen or helium, and the temperature increased in 20 °C increments. The spectra obtained are given in Figure 1b) for H_2/He and 1d) for He.

Under reducing conditions, the nitride phase is lost immediately. The broadening of the white line is lost, however a small residual energy shift of around 0.3 eV remains. The stability is higher in helium, and the intensity and position of the white line begin to shift back towards that of Pd(0) as temperature is increased, indicating the decomposition to the reduced metal. Initial decomposition and loss of lattice nitrogen is rapid, and the shift towards Pd(0) is already substantial by 120 °C. The decomposition is more gradual as the temperature is increased further, reaching a plateau from 160 °C, Figure 1c).

After decomposition of PdN_x the position of the maximum whiteline intensity did not return to the value associated with Pd(0). This change was found for decomposition processes in both H_2/He and He. These residual changes to the Pd NPs following decomposition may indicate legacy effects, and would be particularly important as Pd is often used as a catalyst in processes where the conditions for nitride, carbide and/or hydride formation can be experienced during operation. However two separate previous studies have shown a metallic Pd^0 bond distance can be recovered following PdN_x formation. Decarolis *et al.* found that, whilst the XANES had features of the PdN_x, the EXAFS were consistent with Pd^0, suggesting the remaining nitride is limited to the surface region.[32] Similarly Dann *et al.* were able to achieve reproducible metallic XAFS spectra after *operando* catalytic investigations of the nitride by following a reduction, oxidation then reduction pretreatment.[31] Therefore it is likely that the shift in whiteline position of Pd^0 observed here also relates to surface and subsurface nitrides, rather than irreversible change to the NP structure.

The potential influence of particle size warrants further discussion. The structural properties of PdH_x, specifically the lattice size of the α and β hydride phases, depend on Pd NP size.[37,38] Size effects have also been shown for PdC_x, although only inferred via effects on the conversion and activity of reactions proposed to proceed via *in situ* formation of a PdC_x phase.[20] The studies by Tew *et al.*, where PdC_x formation was observed *in situ* by XAS for samples with a range of Pd particle size, found no correlation.[12,18] Whilst no comprehensive study of size effects PdN_x formation has yet been undertaken, successful PdN_x formation was achieved by *Dann et al.* on both a Pd/γ-Al_2O_3 sample and Pd/zeolite-Y, with particle sizes 2.1 and 5.2 nm respectively.[31] Therefore within the small particle size range typically required for catalytic application, no significant particle size effects are expected.

Formation and stability of palladium carbide, PdC_x

To form palladium carbide, a fresh sample of catalyst was reduced, then exposed to 5% C_2H_4/He at 200 °C, and cooled under He. For the stability tests, again the gas was switched to either diluted hydrogen or helium, and the temperature increased in 20 °C increments, to a higher maximum temperature given the higher stability observed. The spectra obtained are given in Figure 1e) for H_2/He and 1f) for He.

Under hydrogen there was an initial loss in whiteline intensity at 100 °C, with the maximum of the whiteline intensity shifting to lower energies from 140 °C. However, the data remain broadly consistent with PdC_x throughout, with no indication of the complete decomposition of PdC_x to Pd(0). Under He, the features associated with PdC_x were maintained throughout the study, to the maximum temperature of 200 °C. Ziemecki proposed a PdC_x decomposition temperature of $>$600 °C in an inert atmosphere, and of around 150 °C under hydrogen or oxygen.[26] Furthermore, Tew found the palladium carbide phase to be sufficiently stable that under high partial pressures of hydrogen only partial decomposition was observed.[28] The energy shift of the maximum white line intensity, which is observed from 140 °C onwards in the presence of hydrogen, is consistent with a partial decomposition of Pd carbide.

Stability comparison

The incorporation of boron into palladium as an interstitial lattice structure has been considered previously for enhancing the selectivity in alkyne hydrogenation, as an alternative to

Lindlar's catalyst.[21,39–43] As part of the that study, Chan investigated the stability of the PdB_x phase as a function of temperature and gas atmosphere.[21] Whilst PdB_x was formed and tested under different conditions on a different sample, the grouping of boron, carbon and nitrogen in the periodic table, and the conclusions that might be drawn from comparing the three, should not be ignored. Values were also found for palladium hydride under H_2/He from Nag.[36]

Under inert gas (He for the carbide and nitride, N_2 for the boride) the thermal stability of the three phases increases in the order PdN_x*, PdC_x*, PdB_x, with decomposition temperatures of 120, 200+ and 400+ °C respectively (* indicates values originate from this experiment). The same trend occurs under hydrogen; stability increases in the order PdH_x, PdN_x*, PdC_x*, PdB_x, decomposition temperatures 75, ≤100, 140 and 200+°C respectively.

Prior to this work, it was suggested that the stability difference between the boride and the carbide originates from the mixing between the d orbitals of the Pd lattice and the s-p orbitals of the heteroatom. A larger dopant atom would have a higher degree of orbital interaction. The atomic radius increases in the order H<N<C<B, and combining our results with literatures completes the set, giving an order of stability of $PdN_x < PdC_x < PdB_x$. There are likely to be other factors which need to be considered when comparing these dopants, and the orbitals which overlap will not be equivalent for H as for B, C and N, but regardless, these results confirm a correlation between atomic size and stability of the bulk phases.

Solid state NMR

^{14}N MAS NMR was used to detect the nitrogen atoms within the supported Pd nanoparticles. The nitrides were formed following the same treatment steps as for the XANES experiment, but instead using 0.5% NH_3/He. Figure 2 shows a ^{14}N NMR band at ~324.6 ppm for the nitrided samples. Nitrogen is spin-1, and a sharp signal can only be obtained for nitrogen in a highly symmetrical environment. Electric Field Gradient (EFG) calculations were performed through CASTEP, and NQI assignments agree with those stated above (Figure SI 1).

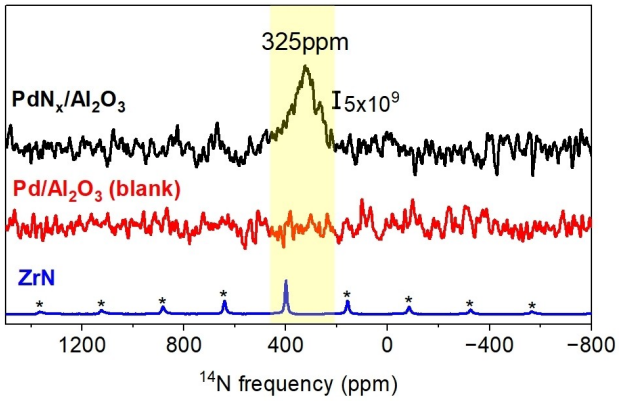

Figure 2. Solid-state ^{14}N NMR spectra (1 s delay) obtained for 1.5 wt% PdN_x/Al_2O_3 and 1.5 wt% Pd/Al_2O_3 blank (with no nitride) measured under the same conditions. Spectra of ZrN with main band at 400 ppm and sidebands (denoted with *) used as a reference for similar nitride systems. V_r = 9 kHz for all spectra, and number of scans (NS) was 404k (PdN/Al_2O_3), 353k (Pd/Al_2O_3), and 16 (ZrN). Intensity scale is shown, and spectra are stacked for clarity.

The NMR experiments on the Pd nitride particles show clearly just one significant signal. The width of the signal reflects small variation in local environment, mostly. There is no evidence of any spinning sidebands, suggesting this is largely originating from interstitial sites. Surface sites may be present in much smaller quantities, beyond detection under the experimental conditions considered here. This technique has been successfully used previously to confirm the integration of boron into a Pd lattice, PdB_x, and to distinguish it from surface boron, using ^{11}B MAS NMR.[21]

DFT modelling of PdN_x formation and decomposition

The above absorption experiments demonstrate the lower stability of the palladium nitride phase compared to the carbide. To try and understand these results further, a DFT computational study was performed. The aim was to compare different mechanisms of Pd nitride decomposition, and hence find the lowest energy route to each.

For this study the truncated octahedral Pd_{38} NP was used, which involves the most common facet [111] of Pd and finite size effects that cannot be captured by slab models. The energy of reaction between different configurations is calculated using the formula in Equation (1):

$$E_{Reaction} = E_{Products} - E_{Reactants} \quad (1)$$

where $E_{Products}$ corresponds to the relaxed structure of products and $E_{Reactants}$ to the relaxed structure of the reactants. For the PdN_x decomposition in an inert atmosphere, the migration of interstitial N to bound surface N has a reaction energy ($E_{Reaction}$) of −84 kJ mol^{-1}, with an activation energy (E_{Act}) of 33.8 kJ mol^{-1}, suggesting that N will eventually migrate and reside on the surface of the NP. Considering the formation of a surface N_2 molecule from two monoatomic nitrogen atoms, each nitrogen atom of the product will be bonded to one palladium atom whilst a predicted $E_{Reaction}$ of −94.4 kJ mol^{-1} for the final N_2 configuration is calculated with an energy barrier E_{Act} equal to 166.1 kJ mol^{-1}. Therefore, the formation of molecular nitrogen from atomic nitrogen on the surface is energetically favoured. The energy of desorption of the N_2 molecule is 19.3 kJ mol^{-1} defined in Equation (2):

$$E_{Desorption} = -E_{Pd_{38}/N_2} + (E_{Pd_{38}} + E_{N_2}), \quad (2)$$

where E_{Pd_{38}/N_2} is the energy of the relaxed system of Pd_{38} including one N_2 molecule, $E_{Pd_{38}}$ is the energy of the perfect NP and E_{N_2} the energy of the N_2 molecule. The proposed mechanism for the decomposition of PdN_x and subsequent formation of molecular nitrogen is displayed visually in Figures 3 and 4, with associated energy values in Table SI1.

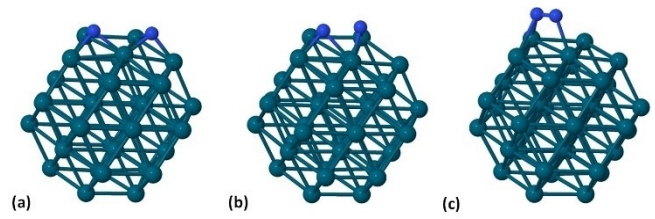

Figure 3. N_2 formation on the [111] facet of Pd_{38} showing the (a) initial, b) transition, and c) final states. Green spheres correspond to Pd atoms and blue spheres to N atoms.

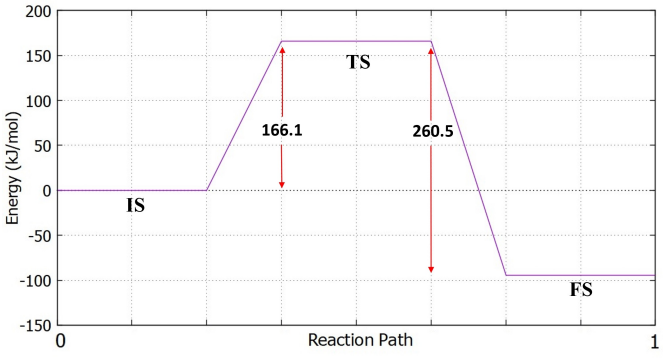

Figure 4. Reaction profile for the formation of N_2 on the [111] facet of Pd_{38}.

For the decomposition of PdN_x in a reducing hydrogen atmosphere there is the alternative that, upon migration to the surface of the NP, atomic nitrogen could gradually bind with atomic hydrogen and desorb as an ammonia molecule. DFT calculations show that the formation of ammonia from surface chemisorbed nitrogen and hydrogen atoms is energetically favoured. The reaction is modelled through three separate steps, Equations (3)–(5):

$$N + H \rightarrow NH \quad (3)$$

$$NH + H \rightarrow NH_2 \quad (4)$$

$$NH_2 + H \rightarrow NH_3 \quad (5)$$

As shown in Figure 5, each separate reaction step is an exothermic process with the lowest $E_{act} = 100.1\ kJ\,mol^{-1}$ corresponding to the formation of *NH*. The associated values of the activation energies are in good agreement with previously reported results on the dehydrogenation of NH_3 on Pd (111) surface, however to our knowledge, the relevant mechanisms on Pd NPs have not yet been investigated.[44–45] Overall, the relaxed structures for each step of the reaction show that the minimum energy configurations for NH_2 and NH_3 are across the edges between [111] facets (Figure 6). Additionally, the bonding of the molecule with surface Pd atoms is reduced as the reaction proceeds along the reaction path showing that NH will bind with three Pd atoms (hollow), NH_2 will bind with two Pd atoms (bridge) and NH_3 with one Pd atom (top).[46] Again, the tabulated energy values corresponding to the each proposed mechanistic step are given in Table SI2.

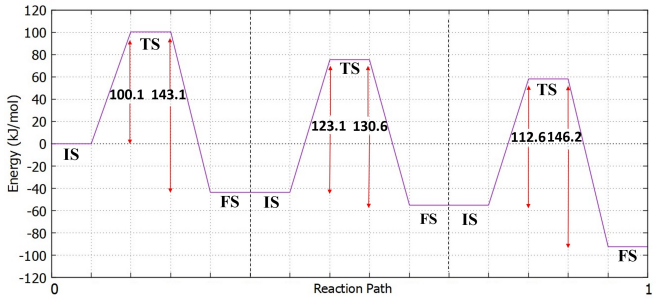

Figure 5. Reaction profile for the formation of NH, NH_2 and NH_3 on the [111] facet of Pd_{38}.

Once NH_3 is formed we assume that it will be desorbed from the Pd_{38} surface. The desorption energy for a single NH_3 molecule corresponds to $132.2\ kJ\,mol^{-1}$ defined by Equation (6):

$$E_{Desorption} = -E_{Pd_{38}/NH_3} + (E_{Pd_{38}} + E_{NH_3}). \quad (6)$$

where E_{Pd_{38}/NH_3} is the energy of the relaxed system of Pd_{38} including one NH_3 molecule, $E_{Pd_{38}}$ is the energy of the perfect NP and E_{NH_3} the energy of the NH_3 molecule.

The complete energy of reaction for the formation of one NH_3 molecule on Pd_{38} is $-84.1\ kJ\,mol^{-1}$ which is less exothermic than the associated value for N_2 formation ($-94.4\ kJ\,mol^{-1}$). However, the higher activation energy barrier for the formation of N_2 on the [111] facet is expected to limit the reaction process and it will be more favourable for Nitrogen to bind with Hydrogen to form *NH*. The calculated energy values for the

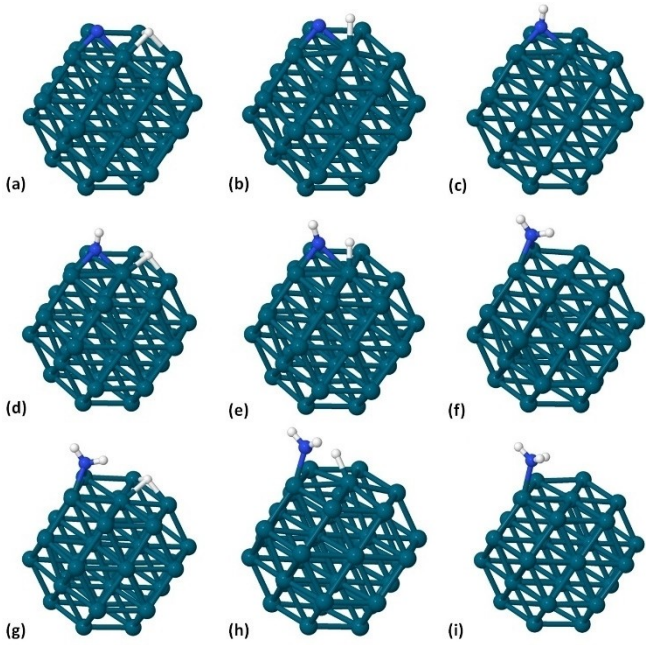

Figure 6. In order, initial, transition, and final states for the formation of (a)–(c) NH (d)–(f) NH_2 and (g)–(i) NH_3 on the [111] facet of Pd_{38}. Green speres correspond to Pd atoms, blue spheres correspond to N atoms and white spheres to H atoms.

nitride decomposition agree with the observations of the XANES experiment, that bulk Pd nitride is unstable.

Conclusions

X-ray absorption spectroscopy experiments have been combined with solid state NMR and computational modelling in this benchmarking experiment on reaction selectivity controlling Pd species. These initial investigations are the first on a path towards utilizing activated species to improve selectivity in reactions where they do not spontaneously form.

PdC_x, PdN_x and PdH_x have been characterized using soft X-rays. Whilst PdH_x has a distinctive spectral feature, those arising in PdC_x and PdN_x are closely matched, suggesting the changes caused to the Pd lattice by their incorporation are very similar. XANES measurements showed PdC_x to be the most stable as a function of temperature and atmosphere. PdN_x however, decomposed immediately on exposure to hydrogen, and began to rapidly decompose under He from 100 °C. Residual differences remained between the decomposed PdN_x and Pd(0), suggesting irreversible structural changes. The presence of an NMR signal at 324.6 ppm using ^{14}N confirms that nitrogen is incorporated into the bulk Pd lattice on formation of PdN_x, not simply adsorbed to the Pd surface.

The decomposition of this nitride requires the breaking of Pd–N bonds and migration of single nitrogen atoms from bulk to surface. From there, we propose the nitrogen desorbs as molecular N_2 in inert atmospheres, and as either N_2 or NH_3 in the present of H_2 gas. Modelling of these mechanisms using DFT suggests a higher barrier to desorption of NH_3 than of N_2, however the activation energy for formation of N_2 is higher and so will likely limit this process.

Experimental Section

XANES. Pd L_3 edge (3175 eV) XANES experiments were performed in fluorescence mode at the XMaS beamline on BM28 at the European Synchrotron Radiation Facility (ESRF). The beam was conditioned using an LN2 cooled Si(111) monochromator, a primary focussing toroidal platinum coated mirror with an angle of incidence of 2.5 mrad and two harmonic rejection mirrors, using stripes of Chromium and Silicon at 3.5 mrad angle of incidence. Both the fluorescence detector and incident beam monitor used were Ketek Silicon drift diodes, fed into a Mercury XIA digital signal processor. The incident beam monitor consists of an in vacuum silicon drift detector exposed to the scatter of the incident X-ray beam from a kapton foil.[33] The *in situ* reactor cell capable of both transmission and fluorescence measurements is described elsewhere (Figure SI2).[34] The cell was mounted vertically in a helium filled stainless steel chamber to reduce absorption of X-rays by air.[34]

XANES data were acquired in step scans from 3155 to 3200 eV. XAS data was collected continuously during each experiment with each scan taking approximately 11 minutes. A reference Pd foil spectrum was acquired periodically during the course of the experiment. The spectra were merged, and analysed using Athena from the Demeter IFEFFIT package.[47]

Synthesis. A 1.5% $Pd/\gamma\text{-}Al_2O_3$ catalyst, prepared by incipient wetness impregnation, was used for all experiments. Prior to the formation of the carbide, nitride and hydride phase, samples were reduced by heating to 120 °C in 3% H_2/He at 25 ml/min for 30 minutes. To form the carbide, the reduced sample was heated to 200 °C in He and held for 10 minutes for temperature stabilisation. 5% C_2H_4/He was flowed at 40 ml/min for 30 min, sample was cooled to 100 °C under reaction gas then held under He. The signal:noise ratio for the carbide data is lower than for the nitride and hydride. The higher carbide formation temperature led to structural issues with the *in situ* cell, and disturbed the window for X-ray transmission. To form the nitride, the reduced sample was held under 40 mL/min 5% NH_3/He at 100 °C for 1 h. To form the hydride, the reduced sample was cooled to 35 °C in 3% H_2/He and held for 30 min. All ramp rates were 5°/min.

For the stability tests, the formed PdN_x and PdC_x were heated from 100 °C in either He or 3% H_2/He in 20 °C increments, allowing 10 min for temperature stabilisation at each temperature. Temperatures were increased until phase decomposition was observed to a maximum of 220 °C.

MAS NMR. NMR experiments were performed on a Bruker Avance Neo widebore Spectrometer, on a 9.4 T wide-bore magnet, using a 5 mm PhoenixNMR probe, tuned to ^{14}N in double resonance mode, with special-made plugins for this application. The scale was calibrated using ammonium chloride as indirect reference, with the ^{14}N peak assigned to 39.3 ppm (compatible with liquid ammonia at 0 ppm).[48] Unless otherwise stated, NMR experiments on ^{14}N consisted of 404000 acquisitions with a flip angle of 30 degrees and a pulse delay of 1 s. Each sample consisted of 95 mg of solid material packed in pencil-style zirconium oxide rotors.

DFT simulations. DFT calculations on the formation of NH_3 and N_2 have been performed with the linear-scaling DFT code ONETEP.[49] Radii of 9.0 Bohr were used for the localized non-orthogonal generalized Wannier functions (NGWFs). A kinetic energy cut-off of 800 eV has been applied for the p-sinc basis-set. The (PBE + D2) exchange correlation functional was used and core electrons were described by norm-conserving relativistic pseudopotentials. The electronic structure has been treated as metallic using the Ensemble-DFT (EDFT) approach with a Fermi-Dirac smearing of 0.1 eV.[50] Geometry optimizations have been performed through the BFGS algorithm. Activation energies have been investigated through the Linear Synchronous Transition / Quadratic Synchronous Transition (LSTQST) protocol.[51] Solid state NMR calculations have been performed through the plane-wave DFT code CASTEP.[52] Geometries have been initially relaxed in vacuum using EDFT with a Fermi-Dirac smearing of 0.1 eV whilst the EFG investigation towards the NQI for interstitial and surface PdN_x have been performed thereafter. A kinetic cut-off of 800 eV has been applied within the PBE + D2 scheme with norm-conserving pseudopotentials.

NMR simulations. SIMPSON spin dynamics calculations were performed to simulate the effect of MAS on the observed signals using the NQI provided by CASTEP.[53,54] Simulations use 10 γ angles, 2000 α, β angles according to the REPULSION scheme, a spin rate of 9 kHz, a non-ideal excitation pulse and a dead time equal to the rotor period, a null chemical shift tensor.[55] The NQI parameters (anisotropy and asymmetry) were taken from the magres CASTEP output file.

The data that support the findings of this study are openly available via the University of Southampton DOI service at https://doi.org/10.5258/SOTON/D2749.

Acknowledgements

XMaS is a UK national research facility supported by EPSRC. We are grateful to all the beamline team staff on BM28 for their support, particularly Paul Thompson. Beamtime award number CH6009. Financial support is acknowledged to the EPSRC (EP/V000691/1) and the UKCP consortium (EP/P022030/1) for access to the ARCHER2 supercomputer. Also to the Materials and Molecular Modelling Hub (EP/T022213/1) and for access to the Young supercomputer, and the University of Southampton for access to the Iridis5 supercomputer. Donato Decarolis and Peter Wells acknowledges funded received through the UK Catalysis Hub and the UK Catalysis Hub is kindly thanked for resources and support provided via our membership of the UK Catalysis Hub Consortium and funded by EPSRC grant: EP/R026815/1, EP/R026939/1, EP/R026645/1 or EP/R027129/1.

Conflict of Interests

The authors declare no conflict of interest.

Keywords: DFT modelling · heterogeneous catalysts · nanoparticles · operando spectroscopy · palladium nitride

[1] M. Twigg, *Catal. Today* **2011**, *163*, 33–41.
[2] S. Rood, S. Eslava, A. Manigrasso, C. Bannister, *J. Automobile Engineering* **2020**, *234*, 936–949.
[3] B. Makhubela, *Johnson Matthey Technol. Rev.* **2018**, *62*, 4–31.
[4] E. S. K. Why, H. C. Ong, H. V. Lee, W. Chen, N. Asikin-Mijan, M. Varman, W. J. Loh, *Energy* **2022**, *239*, 122017.
[5] M. Douthwaite, X. Huang, S. Iqbal, P. J. Miedziak, G. L. Brett, S. A. Kondrat, J. K, Edwards, M. Sankar, D. W. Knight, D. Bethell, G. J. Hutchings, *Catal. Sci. Technol.* **2017**, *7*, 5284–5293.
[6] S. M. Rogers, C. R. Catlow, C. E. Chan-Thaw, A. Chutia, N. Jian, R. E. Palmer, M. Perdjon, A. Thetford, N. Dimitratos, A. Villa, P. P. Wells, *ACS Catal.* **2017**, *7*, 2266–2274.
[7] A. J. McCue, J. A. Anderson, *Chem. Sci. Eng.* **2015**, *9*, 142–153.
[8] R. Chinchilla, C. Nájera, *Chem. Rev.* **2014**, *114*, 1783–1826.
[9] P. Devendar, R. Qu, W. Kang, B. He, G. Yang, *J. Agric. Food Chem.* **2018**, *66*, 8914–8934.
[10] B. Chen, U. Dingerdissen, J. G. E. Krauter, H. G. J. Lansink Rotgerink, K. Möbus, D. J. Ostgard, P. Panster, T. H. Riermeier, S. Seebald, T. Tacke, H. Trauthwein, *Appl. Catal. A* **2005**, *280*, 17–46.
[11] J. Nilsson, P. A. Carlsson, S. Fouladvand, N. M. Martin, J. Gustafson, M. A. Newton, E. Lundgren, H. Grönbeck, M. Skoglundh, *ACS Catal.* **2015**, *5*, 2481–2489.
[12] M. W. Tew, M. Nachtegaal, M. Janousch, T. Huthwelker, J. A. van Bokhoven, *Phys. Chem. Chem. Phys.* **2012**, *14*, 5761–5768.
[13] D. Teschner, J. Borsodi, A. Wootsch, Z. Révary, M. Hävecker, A. Knop-Gericke, S. Jackson, R. Schlögl, *Science* **2008**, *320*, 86–89.
[14] D. Teschner, Z. Révay, J. Borsodi, M. Hävecker, A. Knop-Gericke, R. Schlögl, D. Milroy, S. D. Jackson, D. Torres, P. Sautet, *Angew. Chem. Int. Ed.* **2008**, *47*, 9161–9355.
[15] M. Morkel, G. Rupprechter, H. Freund, *Surf. Sci.* **2005**, *588*, L209–L219.
[16] D. E. Doronkin, S. Wang, D. I. Sharapa, B. J. Deschner, T. L. Sheppard, A. Zimina, F. Studt, R. Dittmeyer, S. Behrens, J. D. Grunwaldt, *Catal. Sci. Technol.* **2020**, *10*, 4726–4742.
[17] N. A. Khan, S. Shaikhutdinov, H. J. Freund, *Catal. Lett.* **2006**, *108*, 159–164.
[18] M. W. Tew, M. Janousch, T. Huthwelker, J. A. van Bokhoven, *J. Catal.* **2011**, *283*, 45–54.
[19] M. Armbrüster, M. Behrens, F. Cinquini, K. Föttinger, Y. Grin, A. Haghofer, B. Klötzer, A. Knop-Gericke, H. Lorenz, A. Ota, S. Penner, J. Prinz, C. Rameshan, Z. Révay, D. Rosenthal, G. Rupprechter, P. Sautet, R. Schlögl, L. Shao, L. Szentmiklósi, D. Teschner, D. Torres, R. Wagner, R. Widmer, G. Wowsnick, *ChemCatChem* **2012**, *4*, 1048–1063.
[20] A. Borodziński, G. C. Bond, *Catal. Rev. Sci. Eng.* **2006**, *48*, 91–144.
[21] W. A. Chan, A. H. Mahadi, M. M. Li, E. C. Corbos, C. Tang, G. Jones, W. C. H. Kuo, J. Cookson, C. M. Brown, P. T. Bishop, S. C. E. Tsang, *Nat. Commun.* **2014**, *5*, 5787.
[22] N. Seriani, F. Mittendorfer, G. Kresse, *J. Chem. Phys.* **2010**, *132*, 024711.
[23] A. A. Skorynina, A. A. Tereshchenko, O. A. Usoltsev, A. L. Bugaev, K. A. Lomachenko, A. A. Guda, E. Groppo, R. Pellegrini, C. Lamberti, A. V. Soldatov, *Radiat. Phys. Chem.* **2020**, *175*, 108079.
[24] A. L. Bugaev, A. G. Guda, I. A. Pankin, E. Groppo, R. Pellegrini, A. Longo, A. V. Soldatov, C. Lamberti, *Catal. Today* **2019**, *336*, 40–44.
[25] A. Kordatos, K. Mohammed, R. Vakili, A. Goguet, H. Manyar, E. Gibson, M. Carravetta, P. Wells, C. Skylaris, *RSC Adv.* **2023**, *13*, 5619–5626.
[26] S. B. Ziemecki, G. A. Jones, D. G. Swartzfager, R. L. Harlow, *J. Am. Chem. Soc.* **1985**, *107*, 4547–4548.
[27] A. L. Bugaev, A. A. Guda, A. Lazzarini, K. A. Lomachenko, E. Groppo, R. Pellegrini, A. Piovano, H. Emerich, A. v. Soldatov, V. P. Dmitriev, J. A. van Bokhoven, C. Lamberti, *Catal. Today* **2017**, *283*, 119–126.
[28] M. W. Tew, J. T. Miller, J. A. van Bokhoven, *J. Phys. Chem. C* **2009**, *113*, 15140–15147.
[29] M. García-Mota, B. Bridier, J. Pérez-Ramírez, N. López, *J. Catal.* **2010**, *273*, 92–102.
[30] R. W. F. Morel, G. C. Williams, F. E. Ryerson, *A study of selected metallic borides, nitrides and phosphides, for the Office of Naval Research*, by University of Louisville Institute of Industrial Research, Kentucky, **1952**, 1–27.
[31] E. K. Dann, E. K. Gibson, R. H. Blackmore, C. R. A. Catlow, P. Collier, A. Chutia, T. E. Erden, C. Hardacre, A. Kroner, M. Nachtegaal, A. Raj, S. M. Rogers, S. F. R. Taylor, P. Thompson, G. F. Tierney, C. D. Zeinalipour-Yazdi, A. Goguet, P. P. Wells, *Nat. Catal.* **2019**, *2*, 157–163.
[32] D. Decarolis, A. H. Clark, T. Pellegrinelli, M. Nachtegaal, E. W. Lynch, C. R. A. Catlow, E. K. Gibson, A. Goguet, P. P. Wells, *ACS Catal.* **2021**, *11*, 2141–2149.
[33] P. Thompson, O. Bikondoa, L. Bouchenoire, S. Brown, M. Cooper, T. Hase, C. Lucas, D. Wermeille, *AIP Conf. Proc.* **2019**, *2054*, 060030.
[34] P. B. J. Thompson, B. N. Nguyen, R. Nicholls, R. A. Bourne, J. B. Brazier, K. R. J. Lovelock, S. D. Brown, D. Wermeille, O. Bikondoa, C. A. Lucas, T. P. A. Hase, M. A. Newton, *J. Synchrotron Radiat.* **2015**, *22*, 1426–1439.
[35] D. M. Nace, J. G. Aston, *J. Am. Chem. Soc.* **1957**, *79*, 3619–3623.
[36] N. K. Nag, *J. Phys. Chem. B* **2001**, *105*, 5945–5949.
[37] M. Suleiman, N. M. Jisrawi, O. Dankert, M. T. Reetz, C. Bähtz, R. Kirchheim, A. Pundt, *J. Alloys Compd.* **2003**, *356–357*, 644–648.
[38] B. Ingham, M. F. Toney, S. C. Hendy, T. Cox, D. D. Fong, J. A. Eastman, P. H. Fuoss, K. J. Stevens, A. Lassesson, S. A. Brown, M. P. Ryan, *Phys. Rev. B* **2008**, *78*, 245408.
[39] J. S. Yoo, Z. Zhao, J. K. Norskøv, F. Studt, *ACS Catal.* **2015**, *5*, 6579–6586.
[40] B. Yang, R. Burch, C. Hardacre, P. Hu, P. Hughes, *J. Phys. Chem. C* **2014**, *118*, 3664–3671.
[41] Z. Li, W. Wei, H. Li, S. Li, L. Leng, M. Zhang, J. H. Horton, D. Wang, W. Sun, C. Guo, W. Wu, J. Wang, *ACS Nano.* **2021**, *15*, 10175–10184.
[42] S. Büchele, Z. Chen, E. Fako, F. Krumeich, R. Hauert, O. V. Sofanova, N. López, S. Mitchell, J. Pérez-Ramírez, *Angew. Chem.* **2020**, *132*, 19807–19812.
[43] I. T. Ellis, E. H. Wolf, G. Jones, B. Lo, M. M. Li, A. P. E. York, S. C. E. Tsang, *Chem. Commun.* **2017**, *53*, 601–604.
[44] Z. Jiang, Q. Pan, M. Li, T. Yan, T. Fang, *Appl. Surf. Sci.* **2014**, *292*, 494–499.
[45] J. A. Herron, S. Tonelli, M. Mavrikakis, *Surf. Sci.* **2012**, *606*, 1670–1679.
[46] S. Stolbov, T. S. Rahman, *J. Chem. Phys.* **2005**, *123*, 204716.
[47] B. Ravel, M. Newville, *J. Synchrotron Radiat.* **2005**, *12*, 537–541.
[48] P. Bertani, J. Raya, B. Bechinger, *J. Solid State Nucl. Magn. Reson.* **2014**, *61*, 15–18.
[49] J. C. A. Prentice, J. Aarons, J. C. Womack, A. E. A. Allen, L. Andrinopoulos, L. Anton, R. A. Bell, A. Bhandari, G. A. Bramley, R. J. Charlton, R. J. Clements, D. J. Cole, G. Constantinescu, F. Corsetti, S. M. M. Dubois, K. K. B. Duff, J. M. Escartín, A. Greco, Q. Hill, L. P. Lee, E. Linscott, D. D. O'Regan, M. J. S. Phipps, L. E. Ratcliff, Á. R. Serrano, E. W. Tait, G. Teobaldi, V. Vitale, N. Yeung, T. J. Zuehlsdorff, J. Dziedzic, P. D. Haynes, N. D. M. Hine, A. A. Mostofi, M. C. Payne, C. K. Skylaris, *J. Chem. Phys.* **2020**, *152*, 174111.
[50] Á. Ruiz-Serrano, C. K. Skylaris, *J. Chem. Phys.* **2013**, *139*, 054107.

[51] N. Govind, M. Petersen, G. Fitzgerald, D. King-Smith, J. Andzelm, *Comput. Mater. Sci.* **2003**, *28*, 250–258.
[52] S. J. Clark, M. D. Segall, C. J. Pickard, P. J. Hasnip, M. J. Probert, K. Refson, M. C. Payne, *Z. Kristallogr.* **2005**, *220*, 567–570.
[53] M. Bak, J. T. Rasmussed, N. C. Nielsen, *J. Magn. Reson.* **2000**, *147*, 296–330.
[54] Z. Tošner, R. Andersen, B. Stevensson, M. Edén, N. C. Nielsen, T. Vosegaard, *J. Magn. Reson.* **2014**, *246*, 79–93.
[55] M. Bak, N. C. Nielsen, *J. Magn. Reson.* **1997**, *125*, 132–139.

Manuscript received: July 12, 2023
Revised manuscript received: August 23, 2023
Accepted manuscript online: September 7, 2023
Version of record online: ■■, ■■

RESEARCH ARTICLE

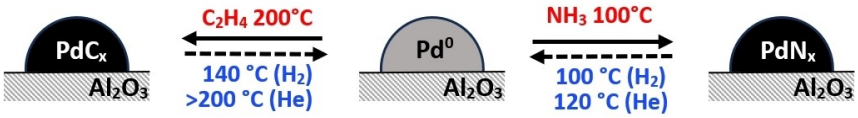

Three interstitial structures of palladium which can form under reactive conditions, PdN_x, PdCx, and PdH_x, have been characterised using in situ X-ray absorption spectroscopy. The thermal stability of the carbide and nitride under both inert and reducing conditions were assessed. Solid-state NMR and DFT measurements were performed for palladium nitride to further unravel its structure and stability.

L. G Costley-Wood, Dr. K. Mohammed, Dr. M. Carravetta, Dr. D. Decarolis, Prof. A. Goguet, Dr. A. Kordatos, Dr. R. Vakili, Dr. H. Manyar, E. McPake, Prof. C.-K. Skylaris, P. Thompson, Dr. E. K Gibson, Dr. P. P. Wells**